J Supercond Nov Magn (2017) 30:2081–2089
DOI 10.1007/s10948-017-4009-5

ORIGINAL PAPER

Prediction of Magnetocaloric Effect by a Phenomenological Model and Critical Behavior for $La_{0.78}Dy_{0.02}Ca_{0.2}MnO_3$ Compound

K. Riahi[1] · I. Messaoui[1] · W. Cheikhrouhou-Koubaa[1] · S. Mercone[2] · B. Leridon[3] · M. Koubaa[1] · A. Cheikhrouhou[1]

Received: 28 January 2017 / Accepted: 3 February 2017 / Published online: 16 February 2017

Abstract The $La_{0.78}Dy_{0.02}Ca_{0.2}MnO_3$ (LDCMO) compound prepared via high-energy ball-milling (BM) presents a ferromagnetic-to-paramagnetic transition (FM-PM) and undergoes a second-order phase transition (SOFT). Based on a phenomenological model, magnetocaloric properties of the LDCMO compound have been studied. Thanks to this model, we can predict the values of the magnetic entropy change ΔS, the full width at half-maximum δT_{FWHM}, the relative cooling power (RCP), and the magnetic specific heat change ΔC_p for our compound. The significant results under 2 T indicate that our compound could be considered as a candidate for use in magnetic refrigeration at low temperatures. In order to further understand the FM-PM transition, the associated critical behavior has been investigated by magnetization isotherms. The critical exponents estimated by the modified Arrott plot, the Kouvel–Fisher plot, and the critical isotherm technique are very close to those corresponding to the 3D-Ising standard model ($\beta = 0.312 \pm 0.07$, $\gamma = 1.28 \pm 0.02$, and $\delta = 4.80$).Those results revealed a long-range ferromagnetic interaction between spins.

Keywords Perovskite · 3D-Ising model · Magnetocaloric properties

✉ K. Riahi
Kalthoumriahi@gmail.com

[1] LT2S Lab (LR16 CRNS 01), Digital Research Center of Sfax, Sfax Technopark, Cité El Ons, B.P. 275, 3021, Sfax, Tunisia

[2] LSPM (UPR 3407) CNRS, Université Paris 13, Sorbonne Paris Cité, 99 Avenue J.-B. Clément, 93430, Villetaneuse, France

[3] LPEM (UPR A0005) CNRS, ESPCI ParisTech, 10 Rue Vauquelin, F-75231, Paris CEDEX 5, France

1 Introduction

Rare earth manganites with a general formula of $R_{1-x}A_xMnO_3$(R = rare earths, A = alkaline earth or alkali elements) gained the attention of researchers due to their interesting electric transport and magnetic properties [1, 2]. The close relation between transport and magnetism in this kind of materials has been explained by many theories, such as double exchange (DE) interaction [3], polaronic effects, [4], and phase separation [5]. Strong competition between lattice, charge, orbital, and magnetic degrees of freedom determines the properties of the perovskites manganites, which lead to a series of novel behaviors related to basic concepts in modern physics and materials science [6, 7]. Today, the universality class of the paramagnetic (PM) to ferromagnetic (FM) transition in manganites is still a controversial question [8]. Previous studies on the critical behaviors and the universality class of the Curie temperature (T_C) transition have indicated that the critical exponents play important roles in elucidating interaction mechanisms near T_C [10, 11].

In this paper, we decided to study the $La_{0.78}Dy_{0.02}Ca_{0.2}MnO_3$ (LDCMO) manganite compound elaborated using a new synthesis route, the ball-milling (BM) process. Experimental details of the BM elaboration have been detailed in our previous work [14]. This method has been known as a very versatile technique to prepare supersaturated solid solutions and other metastable systems, including rare earth (RE) and transition metal (TM)-based systems [12]. The use of BM can be found in literature as a single-step production technique even if annealing maybe necessary sometimes to produce the desired phase [13]. Based on a phenomenological model, we predicted the critical phenomena parameters behavior near the phase transition such as the magnetic entropy change, the relative cooling power (RCP), and the heat capacity. This study allowed estimating

the critical exponents for LDCMO near the Curie temperature. Three different methods have been used to analyze them.

2 Theoretical Consideration

In thermodynamic theory [15], the entropy change ΔS_M associated with a magnetic field variation is given by:

$$\Delta S_M = \int_{0\ \max}^{H} \left(\frac{\partial S}{\partial H}\right)_T dH \tag{1}$$

From Maxwell's thermodynamic lows, it can be written as:

$$\left(\frac{\partial M}{\partial T}\right)_H = \left(\frac{\partial S}{\partial H}\right)_T \tag{2}$$

From (1) and (2):

$$\Delta S_M = \int_0^{H_{\max}} \left(\frac{\partial M}{\partial T}\right)_H dH \tag{3}$$

As a consequence, numerical evaluation of magnetic entropy change can be carried out from (3) using isothermal magnetization measurements.

Hamad [16, 17] has proposed a new model to evaluate magnetic materials behavior by using electrocaloric modeling. The proposed model assumes the temperature dependence of magnetization to be expressed as:

$$M = \frac{(M_i - M_f)}{2} \tanh\left[A\left(T_C - T\right)\right] + BT + C \tag{4}$$

where

M_i is the initial magnetization at FM-PM transition;
M_f is the final magnetization at FM-PM transition;
B is the magnetization sensitivity (dM/dT) in the ferromagnetic region before the transition; and
S_C is the magnetization sensitivity (dM/dT) at Curie temperatureT_C;
$C = \left(\frac{M_i + M_f}{2}\right) - BT_c$;
$A = \frac{(2B - S_C)}{(M_i - M_f)}$.

The magnetic entropy change of a magnetic system under adiabatic magnetic field variation can be evaluated by [16]:

$$\Delta S_M = \left\{-A\left(\frac{M_i - M_f}{2}\right)\mathrm{sech}^2[A\left(T_c - T\right)] + B\right\}\mu_0 H_{\max} \tag{5}$$

At $T = T_C$, the entropy change reaches its maximum; so, (5) may be written as follows [16]:

$$\Delta S_{\max} = \left[-\left(\frac{M_i - M_f}{2}\right) + B\right]\mu_0 H_{\max} \tag{6}$$

The full width at half maximum, δT_{FWHM}, is determined at the two extreme points of the $\Delta S_{\max}$ curves where $\Delta S_{\max}$ is the half of its maximum value. Thus [16]:

$$\delta T_{\mathrm{FWHM}} = \frac{2}{A}\mathrm{sech}\left[\sqrt{\frac{2A\left(M_i - M_f\right)}{A\left(M_i - M_f\right) + 2B}}\right] \tag{7}$$

Thanks to these parameters, the relative cooling power (RCP) can be calculated allowing the evaluation of the magnetocaloric efficiency of the materials. In fact, the RCP is defined as [17]:

$$\begin{aligned}\mathrm{RCP} &= -\Delta S(T, H_{\max}) \times \delta T_{\mathrm{FWHM}} \\ &= (M_i - M_f - 2\frac{B}{A}) H_{\max} \times \mathrm{sech}\left[\sqrt{\frac{2A\left(M_i - M_f\right)}{A\left(M_i - M_f\right) + 2B}}\right]\end{aligned} \tag{8}$$

The heat capacity can be also calculated from the magnetic contribution to the entropy change by the following expression [16]:

$$\Delta C_{p,H} = T\frac{\delta \Delta S_M}{\delta T} \tag{9}$$

According to this model [16], $\Delta C_{p,H}$ can be rewritten as:

$$\begin{aligned}\Delta C_{p,H} = &-TA^2\left(M_i - M_f\right)\mathrm{sech}^2\left[A\left(T_C - T\right)\right] \\ &\times \tanh\left[A\left(T_C - T\right)\right] H_{\max}\end{aligned} \tag{10}$$

3 Scaling Analysis

In accordance with the scaling hypothesis [9], the critical behavior of a magnetic system showing a second-order magnetic phase transition near the Curie point is characterized by a set of critical exponents: the spontaneous magnetization exponent (β), the isothermal magnetic susceptibility exponent (γ), and the critical isotherm exponent (δ). The mathematical definitions of the critical exponents from magnetization measurements are given as follows [18]:

$$M_S = \lim_{H\to 0}(M) = \mathrm{M}_0(-\varepsilon)^{\beta}, \varepsilon < 0\mathrm{T} < T_C \tag{11}$$

$$\chi_0^{-1} = \lim_{H\to 0}(\mu_0 H/M) = (h_0/m_0)\varepsilon^{\gamma}, \varepsilon > 0 \quad T > T_C \tag{12}$$

$$M = D(\mu H)^{1/\gamma}\varepsilon = 0 \quad T = T_C \tag{13}$$

where M_0, h_0, and D are the critical amplitudes and $\varepsilon = (T - T_C)/T_C$ is the reduced temperature. Furthermore, the field and temperature dependence of magnetization in the

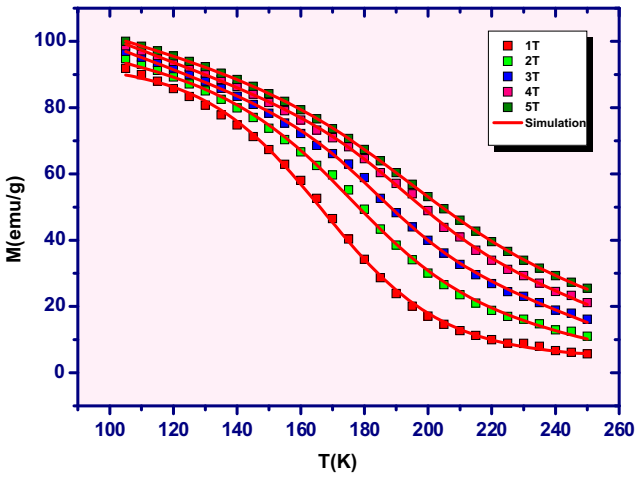

Fig. 1 Temperature dependence of the LDCMO magnetization for different applied magnetic field. *Symbols* represent the experimental data and *solid lines* the simulation obtained by the model in [16]

critical regime obeys to a scaling relation which can be expressed as:

$$M(\mu_0 H, \varepsilon) = (\varepsilon)^{\beta} f_{+-}(\mu_0 H/\varepsilon^{\beta+\gamma}) \tag{14}$$

where f_+ and f_- are regular analytical functions above and below T_C [19, 20]. According to this scaling low, the plots of $M/(\varepsilon)^{\beta}$ versus $H/\varepsilon^{\beta+\gamma}$ would lead to two universal curves: *one* for $T>T_C(\varepsilon>0)$ and the other for $T<T_C(\varepsilon<0)$.

4 Results and Discussion

4.1 Simulation

Based on the phenomenological model proposed by M. A. Hamad [16], we can easily predict the magnetocaloric properties in a magnetic material. First of all, the experimental magnetization data $M(T)$ are fitted using (4) for several magnetic applied fields between 1 and 5 T. In Fig. 1, we report the measured magnetization (symbols) and the simulation (solid line) obtained by using the model parameters given in Table 1. The results of simulation are in very good agreement with the experimental data indicating the accuracy of the method. As shown in Fig. 1, the ferromagnetic to paramagnetic transition is characterized by a continuous decreasing of the magnetization around T_C. The observed smooth change in $M(T)$ for different applied magnetic fields indicates that this magnetic phase transition is of second order [14] (Fig. 2).

Using (13), the change of the specific heat (ΔC_P) versus temperature at various magnetic fields is displayed in Fig. 3. It can be seen that ΔC_P goes through an unexpected change of sign in the vicinity of the transition with a positive value below T_C and a negative one above T_C.

Based on the model parameters reported in Table 1 and on (5), the magnetic entropy change ($-\Delta S_M$) has been predicted and it is displayed in Fig. 2. It is found to be positive in the entire temperature range. However, the full-width at half-maximum of magnetic entropy change and the relative cooling power of the present magnetic refrigerants increase with $\Delta(\mu_0 H)$. At 4 T, (LDCMO) compound reached a high value of RCP around 345 (J/kg), which is relatively close to the reported RCP of the Gd material [21] of 535 (J/kg). Thus, our compound can be a good candidate for magnetic refrigeration.

4.2 Critical Exponents

The reliable method used for obtaining the exact values of the critical exponents and critical temperatures is based on the measurement of the magnetic isotherm $M(H)$ curves at various temperatures. The LDCMO magnetization $M(H)$ has been measured with a step of 2 K in the vicinity of Curie temperature as shown in Fig. 4.

4.2.1 Arrott–Noakes Plot or Modified Arrot Plots

The $(M)^{1/\beta}$ versus $(H/M)^{1/\gamma}$ Arrott–Noakes plots [22], also known as modified Arrott plots (MAP), are constructed for the LDCMO compound using four different kinds of trial exponents. Based on the magnetic state equation:

$$\left(\frac{H}{M}s\right)^{1/\gamma} = \frac{a(T-T_C)}{T}\mathrm{g} + bM^{1/\beta} \tag{15}$$

where a and b are considered to be constants.

Table 1 LDCMO parameters from (4) at different applied magnetic fields (see text)

$\mu_0 H(T)$	M_i (emu/g)	M_f (emu/g)	T_C (K)	B (emu g^{-1}K^{-1})	R^2
1	86.592 (2)	0.924 (8)	166.886 (1)	−0.016 (6)	0.999 (4)
2	77.210 (4)	18.901 (8)	175.850 (2)	−0.187 (6)	0.998 (9)
3	71.622 (6)	40.760 (7)	184.116 (3)	−0.353 (2)	0.999 (4)
4	73.217 (7)	45.782 (3)	193.105 (8)	−0.356 (6)	0.999 (8)
5	82.208 (5)	42.391 (8)	194.441 (7)	−0.265 (4)	0.999 (8)

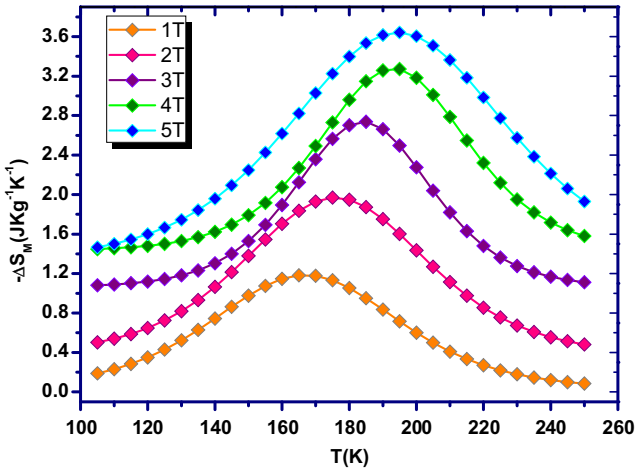

Fig. 2 Magnetic entropy change, $(-\Delta S_M)$ versus temperature for different magnetic fields

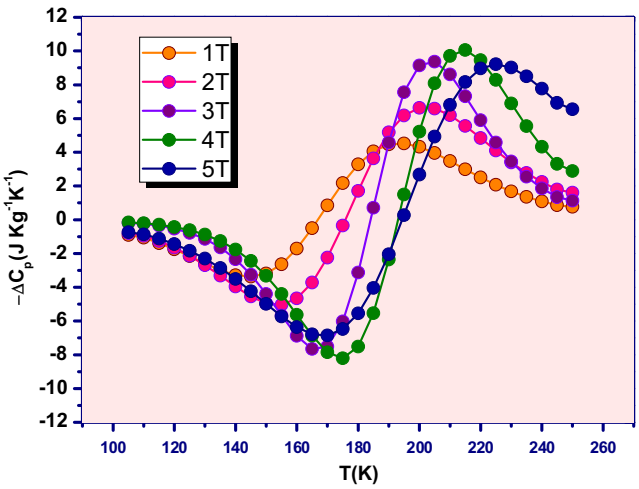

Fig. 3 Heat capacity changes as function of temperature for different applied magnetic field

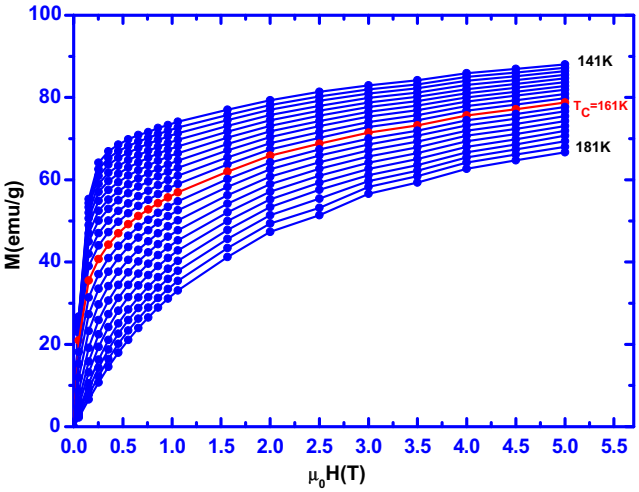

Fig. 4 Isothermal magnetization curves

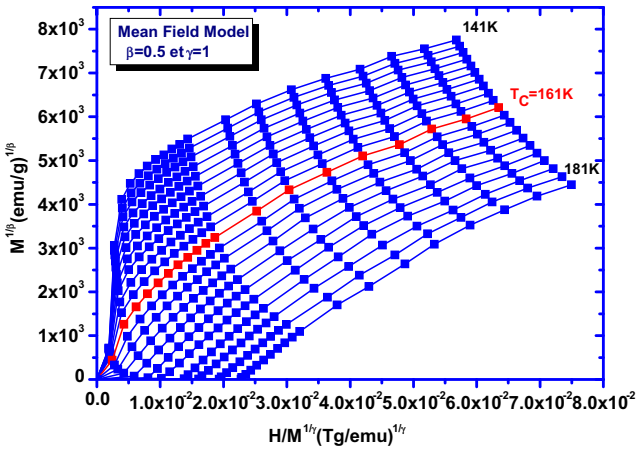

Fig. 5 Modified Arrott plots (MAP): isotherms of $M^{1/\beta}$ versus $\mu_0 H/M^{1/\gamma}$ by the mean–field model

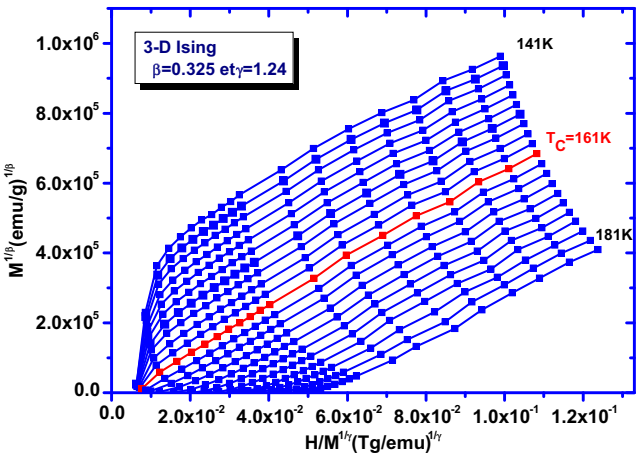

Fig. 6 Modified Arrott plots (MAP): isotherms of $M^{1/\beta}$ versus $\mu_0 H/M^{1/\gamma}$ by the 3D-Ising model

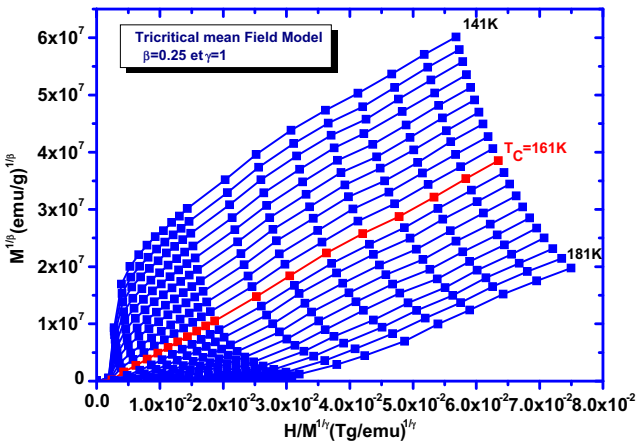

Fig. 7 Modified Arrott plots (MAP): isotherms of $M^{1/\beta}$ versus $\mu_0 H/M^{1/\gamma}$ by the tricritical mean–field model

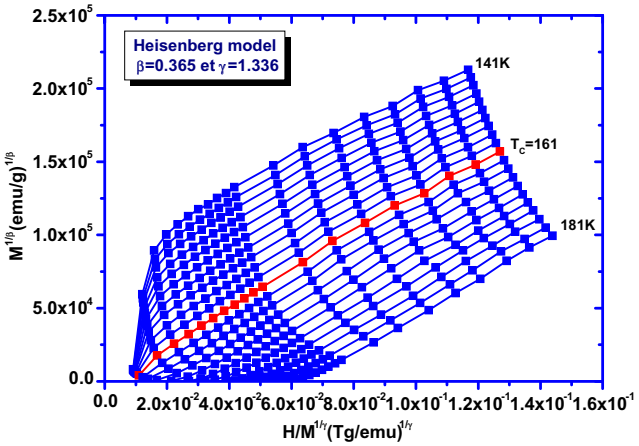

Fig. 8 Modified Arrott plots (MAP): isotherms of $M^{1/\beta}$ versus $\mu_0 H/M^{1/\gamma}$ by the 3D-Heisenberg model

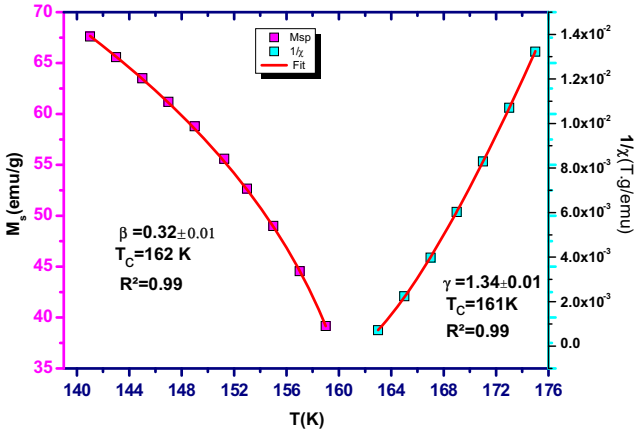

Fig. 10 The spontaneous magnetization $M_S(T)$ (*left axis*) and the initial inverse susceptibility $\chi^{-1}(T)$ (*right axis*) together with the fitting curves (*solid lines*)

In theory, we have four kinds of trial exponents that are used to plot the MAP by using four models of critical exponents: mean–field model ($\beta = 0.5$ and $\gamma = 1$); 3D Heisenberg model ($\beta = 0.365$ and $\gamma = 1.336$); 3D-Ising model ($\beta = 0.325$ and $\gamma = 1.24$) and tricritical mean–field model ($\beta = 0.25$ and $\gamma = 1$) as shown in Figs. 5, 6, 7 and 8.

In these four models, the lines in the high field region are quasi-parallel, so it is complicated to distinguish which one of them is the best model to determine the critical exponents. Thus, we calculated the so-called relative slope (RS) defined at the critical point as RS $= S(T)/S(T_C)$.The RS of the best model should be near the unity. As shown in Fig. 9, the RS of LDCMO using the mean–field model, the Heisenberg, and the tricritical ones, clearly deviates from 1. On the contrary, the RS of 3D-Ising model is close to unity. Thus, the latter is the best model to describe our perovskite material.

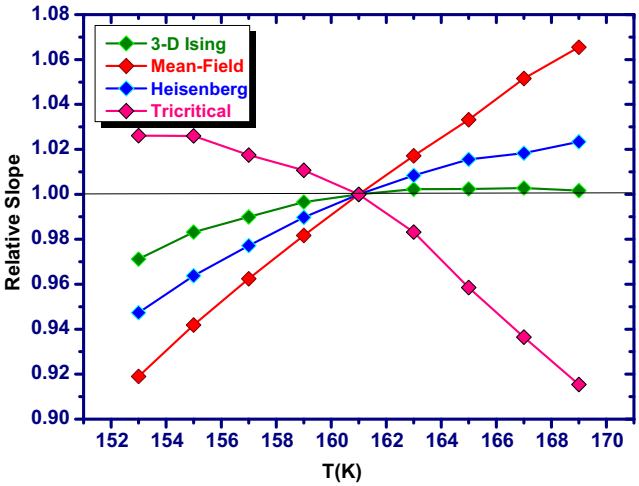

Fig. 9 Relative slope (RS) versus temperature defined by RS $= S(T)/S(T_C)$

Based on the MAP, the spontaneous magnetization $M_S(T)$ as well as the inverse of the magnetic susceptibility $\chi_0^{-1}(T)$ were determined from the intersections of the linear extrapolation line with the $(M)^{1/\beta}$ and the $(H/M)^{1/\gamma}$ axis, respectively. The $M_S(T)$ and $\chi_0^{-1}(T)$ are shown in Fig. 10. Those curves denote the power low fitting of $M_S(T)$ and $\chi_0^{-1}(T)$ according to (1) and (2), respectively. The new critical exponent values were hence determined and reported in Table 2. In addition, the Curie temperatures associated with the fitting of $M_S(T)$ and $\chi_0^{-1}(T)$ with (1) and (2), respectively, are also determined.

4.2.2 Kouvel–Fisher Method

The Kouvel–Fisher (KF) method is the most accurate procedure to determinate the critical exponents. It is based on the following equations [23]:

$$M_S(T)[dM_S(T)/d(T)]^{-1} = 1/\beta(T - T_C) \tag{16}$$

$$\chi_0^{-1}(T)[d\chi_0^{-1}(T)/dT]^{-1} = 1/\gamma(T - T_C) \tag{17}$$

According to (16) and (17), plots of $M_S(T)[dM_S(T)/d(T)]^{-1}$ and $\chi_0^{-1}(T)[d\chi_0^{-1}(T)/dT]^{-1}$ versus temperature should yield to straight lines with $1/\beta$ and $1/\gamma$ as slopes, respectively, and with intercepts on T axes equal to Curie temperature (T_C). In Fig. 11 the critical exponents obtained from the KF methods are $\beta = 0.312 \pm 0.007$ and $\gamma = 1.28 \pm 0.02$.

It is easy to remark that the critical exponents values as well as T_C calculated by the MAP and KF-plots, match reasonably well.

Table 2 Comparison of ΔS_{max}, RCP, and ΔC_p for LDCMO and related materials

Materials	$\mu_0 H$ (T)	ΔS_{max} (J kg K)	δT_{FWHM} (K)	RCP (J kg)	$\Delta C_{p,H}^{max}$ (J kg K)	$\Delta C_{p,H}^{min}$ (J kg K)	Ref.
$La_{0.78}Dy_{0.02}Ca_{0.2}MnO_3$	1	1.182(5)	67.698 (0)	80.022 (2)	3.336 (0)	−4.623(2)	Present work
	2	1.968 (9)	78.313 (2)	154.134 (1)	4.95 (1)	−6.711(1)	Present work
	3	2.738 (9)	81.575 (1)	223.367 (2)	7.63 (1)	−9.41(0)	Present work
	4	3.271(9)	105.52(0)	345.207(3)	8.14(2)	−10.06(0)	Present work
Gd	5	10.2	–	410	–	–	[35]
$La_{0.75}Ca_{0.25}MnO_3$	0.5	1.36	19.55	26.5	22.42	−21.11	[36]
	1	2.52	16.71	42.19	59.71	−56.77	[36]
	4	5.39	33.97	183.16	58.11	−53.19	[36]
$La_{0.8}Ca_{0.2}MnO3$	5	5.8	–	280.6	–	–	[37]
$La_{0.8}Ca_{0.05}K_{0.15}MnO_3$	5	5.32	–	236.99	–	–	[37]
$La_{0.8}Ca_{0.05}K_{0.15}MnO_3$	5	5.32	–	236.99	–	–	[37]
$La_{0.8}K_{0.2}MnO_3$	5	4.37	–	241.6	–	–	[37]

4.2.3 Critical Isotherm Exponent

The third critical exponent δ can be determined by plotting the $M(H)$ data at $T = T_C$ according to (13). Based on the obtained critical exponents, the $M(H, T_C = 161\ \text{K})$ versus H measured from 0 to 5 T, were chosen as the critical isothermal magnetizations, as shown in Fig. 12. The inset of the same figure shows the $M(H)$ curve on a log–log scale. From the linear fitting in inset Fig. 12, the value of δ is found to be 4.80. Furthermore, exponent δ has been calculated from Widom scaling relation defined as [24]:

$$\gamma = 1 + \frac{\gamma}{\beta} \tag{18}$$

Using the above scaling relation and estimated values of β and γ from the modified Arrott plot method as shown in Fig. 12, we have obtained $\delta = 4.80$. The δ value deduced from the KF method in Fig. 11 is $\delta = 5.10$. This value is larger than the one estimated from the Widom scaling. This difference is probably due to the experimental errors.

4.2.4 Scaling Law

In Fig. 13, we have plotted $M/|\varepsilon|^{-\beta}$ versus $H/|\varepsilon|^{-(\beta+\gamma)}$ curves with β and γ obtained from the KF method. It is clear that all the data fall into one of the two parts of the plots, i.e., one part for temperatures above T_C ($T > T_C$) and the other for temperatures below T_C ($T < T_C$). To ensure a good visualization of the separation of curves, we plot the curves with log–log scale inset (Fig. 13). This evidently suggests that the obtained values of the critical exponents and the T_C one, confirm the reliability and the good concordance with

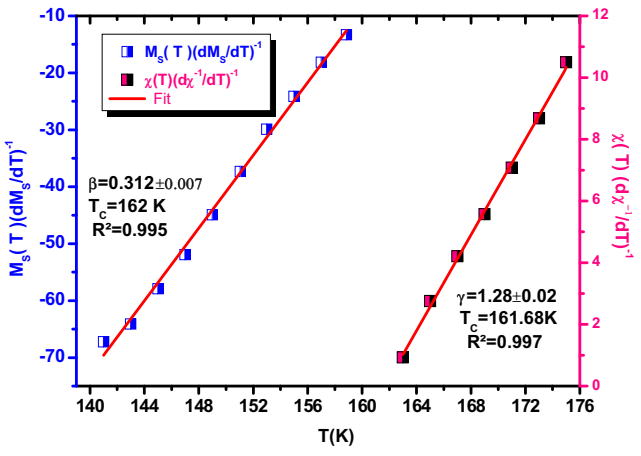

Fig. 11 Kouvel–Fisher plots for the spontaneous magnetization $M_S(T)$ (*left axis*) and the initial inverse susceptibility $\chi_0^{-1}1$ (*right axis*) for LDCMO sample. *Solid lines* correspond to the linear fit of $M_S(T)$ and χ_0^{-1} data

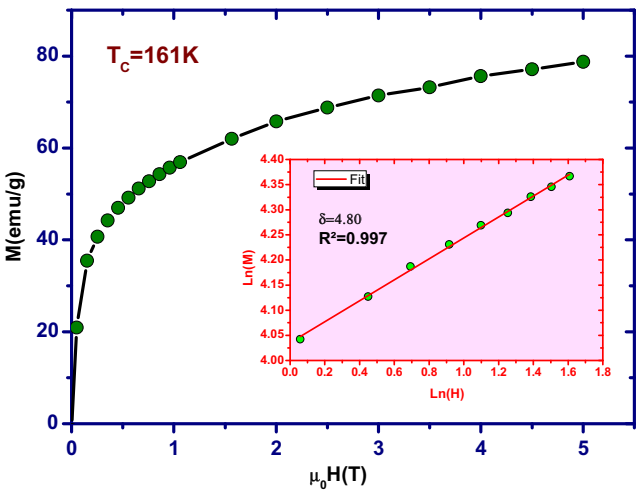

Fig. 12 Isothermal magnetic curves at $T = T_C$. The *inset* shows the plot in a logarithmic scale. The critical exponents mentioned in graph are obtained from the linear fit (*solid line*)

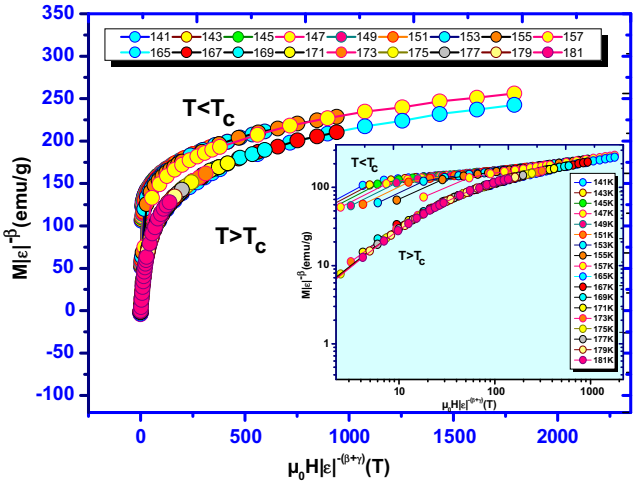

Fig. 13 Scaling plots indicating two universal curves below and above TC for LDCMO sample. The *inset* shows the plot in a log-log scale

the scaling hypothesis. Indeed, all data fall into two distinct branches, one for temperature below T_C and the other for temperature above T_C.

It is obvious that the values of the critical exponents agree well with those of 3-D Ising model, suggesting that the interactions among spins are of short range type. Actually, this is completely accepted for perovskite manganites [25].

As reported above, LDCMO exhibits a large MCE around T_C but it's still useless for a magnetic sensor device designed to work at room temperature [26]. Our results are similar to those of Khlifi et al. [27], in which they found that the critical exponents of $La_{0.8}Ca_{0.2}MnO_3$ agree pretty well with the 3-D Ising model predictions. Therefore, the slight substitution with Dy^{3+} in LDCMO does not affect the universality class.

In another work, Kim et al. [28, 29] pointed out that the critical exponents of the $La_{0.6}Ca_{0.4}MnO3$ contain a tricritical point separating regions of first-order transition from regions of second-order one. These results are not consistent with the LDCMO ones discussed here showing a Dy^{3+} substitution effect. An interesting feature is also that in $La_{1-x}Ca_xMnO_3$compounds, the 3D-Heisenberg model is applicable only for $x < 0.2$. Severe deviations for $x \geq 0.2$ have been observed (in fact, for$x = 0.3$ a first-order transition occurs) [30, 31]. In particular, at $x = 0.2$, the obtained critical exponents are between the 3D-Heisenberg and the 3D-Ising model [29]. At this point, we decided to go further and to compare the critical behavior found in our study with other manganite systems reported in literature (see Table 3).

One of the drawbacks of several studies is that they have been done on polycrystalline samples which present a strong smearing in the phase transitions, making it difficult to evaluate the critical parameters [32]. Numerous papers are dealing with the critical exponents in manganites. For the same composition, we can notice a difference between critical exponents near the transition's temperature depending on the synthesis process used. For instance, Ezaami et al. [33] have studied the effect of synthesis route on the critical behavior of $La_{0.7}Ca_{0.2}Sr_{0.1}MnO_3$ manganite system in the vicinity of the Curie temperature and their results showed a change in the universality class. Moreover, Messaoui et al. [34] noticed that by changing the milling time, the critical behavior changed from the tricritical mean–field prediction

Table 3 Critical exponents for LDCMO compound compared to earlier values reported in literature by using various theoretical models

Materials	Method	β	γ	δ	Ref.
$La_{0.78}Dy_{0.02}Ca_{0.2}MnO_3$	MAP	0.32 ± 0.01	1.34 ± 0.01	–	This work
	KF	0.312 ± 0.007	1.28 ± 0.02	–	This work
	C.I. (cal)	–	–	5.10	This work
	C.I. (exp)	–	–	4.81 ± 0.03	This work
Mean–field model	Theory	0.5	1.0	3.0	[18]
3D-Heisenberg model	Theory	0.365	1.336	4.80	[18]
3D-Ising model	Theory	0.325	1.241	4.82	[18]
Tricritical mean–field model	Theory	0.25	1	5	[18]
$La_{0.7}Ca_{0.2}Sr_{0.1}MnO_3$		0.394 ± 0.008	0.925 ± 0.021	3.34 ± 0.01	[38]
$La_{0.8}Ca_{0.2}MnO_3$		0.316 ± 0.007	1.081 ± 0.036	4.421	[39]
$La_{0.7}Ca_{0.3}MnO_3$		0.36 ± 0.01	1.2	4.33	[40]
$La_{0.6}Ca_{0.4}MnO_3$		0.25 ± 0.03	1.03 ± 0.05	5.0 ± 0.8	[41]
$La_{0.5}Ca_{0.4}Ag_{0.1}MnO_3$		0.311 ± 0.003	1.146 ± 0.006	4.83 ± 0.01	[42]
$La_{0.1}Nd_{0.6}Sr_{0.3}MnO_3$		0.257 ± 0.005	1.12 ± 0.03	5.17 ± 0.02	[43]
$Nd_{0.7}Ca_{0.15}Sr_{0.15}MnO_3$		0.2437 ± 0.01	0.9077 ± 0.041	4.547 ± 0.041	[34]
$La_{0.7}Pb_{0.05}Na_{0.25}MnO_3$		0.344	1.296	4.80	[44]
$Pr_{0.58}Er_{0.02}Ca_{0.1}Sr_{0.3}MO_3$		0.337 9)	1.189 (28)	4.528	[45]

to the 3D-Ising model one in $Nd_{0.7}Sr_{0.15}Ca_{0.15}MnO_3$ polycrystalline sample.

Up to now, although the wide difference of critical phenomena is reported in the literature, it is difficult to determine the common universality class for a continuous PM-FM phase transitions in manganites. The better way for this issue needs more experimental measurements on high purity samples with different compositions [32].

5 Conclusion

In summary, $La_{0.78}Dy_{0.02}Ca_{0.2}MnO_3$ compound was synthesized by high-energy ball-milling process. We simulated the dependence of magnetization, magnetic entropy, and heat capacity change as a function of temperature for (LDCMO) materials under an external magnetic field. A large magnetocaloric effect is observed, and the large relative cooling power (RCP) is found to be 345 (J/kg) under 4 T. Thus, we can consider our sample as a potential candidate for magnetic refrigeration applications. The critical properties of the perovskite manganite were studied using the isothermal magnetization around Curie temperature (T_C), based on various techniques: Arrott plot, Kouvel–Fisher analysis, and critical isotherm method. Furthermore, the validity of our critical exponents was confirmed by the universal scaling analysis. The obtained critical exponents are similar to those predicted by the 3D-Ising.

Acknowledgments This work was supported by the Tunisian Ministry of Higher Education and Scientific Research. The magnetic measurements at ESPCI have been supported through grants from Region Ile-de-France.

References

1. Ramirez, A.P.: Colossal-magnetoresistance. J. Phy: Condens. Matter **9**, 8171–8199 (1997)
2. Nagaev, E.L.: Colossal magnetoresistance materials: manganites and conventional ferromagnetic semiconductors. Phys. Rep. **346**, 387 (2001)
3. Zener, C.: Interaction between d-shells in the transition metals. II. Ferromagnetic compounds of manganese with perovskite structure. Phys. Rev. **82** (1951)
4. Millis, A.J., Littlewood, P.B., Shraiman, B.I.: Double exchange alone does not explain the resistivity of $La_{1-x}Sr_xMnO_3$. Phys. Rev. Lett. **74**, 5144 (1995)
5. Mori, S., Chen, C.H., Cheong, S.W.: Paired and unpaired charge stripes in the ferromagnetic phase of $La_{0.5}Ca_{0.5}MnO_3$. Phys. Rev. Lett. **81**, 3972 (1998)
6. Prinz, G.A.: Spin-polarized transport. Phys. Today **48**, 58 (1995)
7. Tomioka, Y., Asamitsu, A., Moritomo, Y., Kuwahara, H., Tokura, Y.: Collapse of a charge-ordered state under a magnetic field in $Pr_{1/2}Sr_{1/2}MnO_3$. Phys. Rev. Lett. **74**, 5108 (1995)
8. Khiem, N.V., Phong, P.T., Bau, L.V., Nam, D.N.H., Hong, L.V., Phuc, N.X.: Critical parameters near the ferromagnetic-paramagnetic phase transition in La0.7A0.3($Mn_{1-x}b_x$)O3(A = Sr; B = Ti and Al; x = 0.0 and 0.05) compounds. J. Magn. Magn. Mater. **321**, 2027 (2009)
9. Stanley, H.E.: Introduction to phase transitions and critical phenomena. Oxford University Press, London (1971)
10. Phan, M.H., Franco, V., Bingham, N.S., Srikanth, H., Hur, N.H., Yu, S.C.: Tricritical point and critical exponents of $La_{0.7}Ca_{0.3-x}Sr_xMnO_3$ (x = 0, 0.05, 0.1, 0.2, 0.25) single crystals. J. Alloys. Compd. **508**, 238–244 (2010)
11. Zghal, E., Koubaa, M., CheikhrouhouKoubaa, W., Cheikhrouhou, A., Sicard, L., Ammar-Merah, S.: Influence of magnetic field on the critical behavior of $La_{0.7}Ca_{0.2}Ba_{0.1}MnO_3$. J. Alloys. Comp. **627**, 211–217 (2015)
12. Suryanarayana, C.: 'Mechanical alloying and milling'. Prog. Mater. Sci. **46**(1), 184 (2001)
13. Blazquez, J.S., ipus, J.J., Moreno-Ramirez, L.M., Borrego, J.M., Lozano-Perez, S., FRANCO, V., CONDE, C.F., CONDE, A.: Analysis of the magnetocaloric effect in powder samples obtained by ball milling. Metall. Mater. Trans. E. **2**, 136 (2015)
14. Riahi, K., Messaoui, I., Cheikhrouhou-Koubaa, W., Mercone, S., Leridon, B., Koubaa, M., Cheikhrouhou, A.: Effect of synthesis route on the structural, magnetic and magnetocaloric properties of $La_{0.78}Dy_{0.02}Ca_{0.2}MnO_3$ manganite: a comparison between sol-gel, high-energy ball-milling and solid state process. J. Alloys. Compd. **688**, 1028–1038 (2016)
15. Phan, M.H., Tian, S.B., Yu, S.C., Ulyanov, A.N.: Magnetic and magnetocaloric properties of $La_{0.7}Ca_{0.3-x}Ba_xMnO_3$ compounds. J. Magn. Magn. Mater. **256**, 306–310 (2003)
16. Hamad, M.A.: Prediction of thermomagnetic properties of $La_{0.67}Ca_{0.33}MnO_3$ and La0.67Sr0.33MnO3. Phase Trans **85**, 106–112 (2012)
17. Hamad, M.A.: Calculation on electrocaloric properties of ferroelectric $SrBi_2Ta_2O_9$. Phase Trans **85**, 159–168 (2012)
18. Fisher, M.E.: The theory of equilibrium critical phenomena. Rep. Prog. Phys. **30**, 615 (1967)
19. Stanley, H.E.: Scaling, universality, and renormalization: three pillars of modern critical phenomena. Rev. Mod. Phys. **71**, 358 (1999)
20. Kaul, S.N.: Thermal modulation studies of the critical magnetic susceptibility of Gd. J. Magn. Magn. Mater. **53**, 5 (1985)
21. Pennington, W.T.: DIAMOND visual crystal structure information system. J. Appl. Cryst. **32**, 1028–1029 (1999)
22. Mira, J., Rivas, J., Hueso, L.E., Rivadulla, F., Lopez-Quintela, M.A.: Tuning of colossal magnetoresistance via grain size change in $La_{0.67}Ca_{0.33}MnO_3$. J. Appl. Phys. **91**, 8903 (2002)
23. Arrot, A., Noakes, J.E.: Approximate equation of state for nickel near its critical temperature. Phys. Rev. Lett. **19**, 786 (1967)
24. Kouvel, J.S., Fisher, M.E.: Detailed magnetic behavior of nickel near its Curie point. Phys. Rev. **136**, A1626 (1964)
25. Widom, B.: Equation of state in the neighborhood of the critical point. J. Chem. Phys. **43**, 3898 (1965)
26. Mohamed, Za., Tka, E., Dhahri, J., Hlil, E.K.: Short-range ferromagnetic order in $La_{0.67}Sr_{0.16}Ca_{0.17}MnO3$ perovskite manganite. J. Alloys. Compd. **619**, 520–526 (2015)
27. Khlifi, M., Tozri, A., Bejar, M., Dhahri, E., Hlil, E.K.: Effect of calcium deficiency on the critical behavior near the paramagnetic to ferromagnetic phase transition temperature in $La_{0.8}Ca_{0.2}MnO_3$oxides. J. Magn. Magn. Mater. **324**, 2142–2146 (2012)
28. Kim, D., Revaz, B., Zink, B.L., Hellman, F., Rhyne, J.J., Mitchell, J.F.: Tricritical point and the doping dependence of the order of the ferromagnetic phase transition of $La_{1-x}Ca_xMnO_3$. Phys. Rev. Lett. **89**, 227202 (2002)

29. Zhang, P., Lampen, P., Phan, T.L., Yu, S.C., Thanh, T.D., Dan, N.H., Lam, V.D., Srikanth, H., Phan, M.H.: Influence of magnetic field on critical behavior near a first order transition in optimally doped manganites: The case of $La_{1-x}Ca_xMnO_3$ ($0.2x0.4$). J. Magn. Magn. Mater. **348**, 146 (2013)
30. Jiang, W., Zhou, X., Williams, G., Mukovskii, Y., Privenzentsev, R.: The evolution of Griffiths-phase-like features and colossal magnetoresistance in $La_{(1-x)}Ca_{(x)}MnO_3$ ($0.18\ x\ 0.27$) across the compositional metal-insulator boundary. J. Phys. Condens. Matter **21**, 415603 (2009)
31. Ferreira, P.M.G.L., Souza, J.A.: Scaling behavior of nearly first order magnetic phase transitions. J. Phys. Condens. Matter **23**, 226003 (2011)
32. Oleaga, A., Salazar, A., CiomagaHantean, M., Balakrishnan, G.: Three-dimensional Ising critical behavior in $R_{0.6}Sr_{0.4}MnO_3$ (R = Pr, Nd) manganites. Phys. Rev. B **92**, 024409 (2015)
33. Ezaami, A., Sfifir, I., Cheikhrouhou-Koubaa, W., Koubaa, M., Cheikhrouhou, A.: Critical properties in La0·7Ca0·2Sr0·1MnO3 manganite: a comparison between sol-gel and solid state process. J. Alloys Comp **693**, 658–666 (2016)
34. Messaoui, I., Omrani, H., Mansouri, M., CheikhrouhouKoubaa, W., Koubaa, M., Cheikhrouhou, A., Hlil, E.K.: Magnetic, magnetocaloric and critical behavior investigation of $Nd_{0.7}Ca_{0.15}Sr_{0.15}MnO_3$ prepared by high-energy ball milling. Ceram. Intern. **42**, 17032–17044 (2016)
35. Phan, M.H., Yu, S.C.: Review of the magnetocaloric effect in manganite materials. J. Magn. Magn. Mater. **308**, 325–340 (2007)
36. Hamad, M.A.: Theoretical work on magnetocaloric effect in $La_{0.75}Ca_{0.25}MnO_3$. J .Adv. Ceram. **1**(4), 290 (2012)
37. Mbarek, H., M'nasri, R., Cheikhrouhou-Koubaa, W., Cheikhrouhou, A.: Magnetocaloric effect near room temperature in (1-y)$La_{0.8}Ca_{0.05}K_{0.15}MnO_3$/y$La_{0.8}K_{0.2}MnO_3$ composites. Phys. Stat. Sol. A. **211**, 975 (2014)
38. Phan, T.L., Zhang, Y.D., Zhang, P., Thanh, T.D., Yu, S.C.: Critical behavior and magnetic-entropy change of orthorhombic $La_{0.7}Ca_{0.2}Sr_{0.1}MnO_3$. J. Appl. Phys. **112**, 093906 (2012)
39. Zhang, P., Lampen, P., Phan, T.L., Yu, S.C., Thanh, T.D., Dan, N.H., Lam, V.D., Srikanth, H., Phan, M.H.: Influence of magnetic field on critical behavior near a first order transition in optimally doped manganites: The case of $La_{1-x}Ca_xMnO_3$ ($0.2x0.4$). J. Magn. Magn. Mater **348**, 146 (2013)
40. Taran, S., Chaudhuri, B.K., Chatterjee, S., Yang, H.D., Neeleshwar, S., Chen, Y.Y.: Critical exponents of the $La_{0.7}Sr_{0.3}MnO_3$, $La_{0.7}Ca_{0.3}MnO_3$, and $Pr_{0.7}Ca_{0.3}MnO_3$ systems showing correlation between transport and magnetic properties. J. Appl. Phys. **98**, 103903 (2005)
41. Kim, D., Revaz, B., Zink, B.L., Hellman, F., Rhyne, J.J., Mitchell, J.F.: Tricritical point and the doping dependence of the order of the ferromagnetic phase transition of $La_{1-x}Ca_xMnO_3$. Phys. Rev. Lett. **89**, 227202 (2002)
42. Smari, M., Walha, I., Omri, A., Rousseau, J.J., Dhahri, E., Hlil, E.K.: Critical parameters near the ferromagnetic–paramagnetic phase transition in $La_{0.5}Ca_{0.5-x}Ag_xMnO_3$ compounds ($0.1x0.2$). Ceram. Int. **40**, 8945 (2014)
43. Fan, J., Ling, L., Hong, B., Zhang, L., Pi, L., Zhang, Y.: Critical properties of the perovskite manganite $La_{0.1}Nd_{0.6}Sr_{0.3}MnO_3$. Phys. Rev. B **81**, 144426 (2010)
44. Motome, Y., Furulawa, N.: Critical temperature of ferromagnetic transition in three-dimensional double-exchange models. J. Phys. Soc. Jap. **69**, 3785–3788 (2000)
45. Omrani, H., Mansouri, M., CheikhrouhouKoubaa, W., Koubaa, M., Cheikhrouhou, A.: Critical behavior study near the paramagnetic to ferromagnetic phase transition temperature in $Pr_{0.6-x}Er_xCa_{0.1}Sr_{0.3}MnO3$ (x = 0, 0.02 and 0.06) manganites. RSC Adv **6**, 78017–78027 (2016)